

Laser-Induced Graphene for Electrothermally Controlled, Mechanically Guided, 3D Assembly and Human-Soft Actuators Interaction


Yun Ling, Wenbo Pang, Xiaopeng Li, Shivam Goswami, Zheng Xu, David Stroman, Yachao Liu, Qihui Fei, Yadong Xu, Ganggang Zhao, Bohan Sun, Jingwei Xie, Guoliang Huang, Yihui Zhang,* and Zheng Yan*

Mechanically guided, 3D assembly has attracted broad interests, owing to its compatibility with planar fabrication techniques and applicability to a diversity of geometries and length scales. Its further development requires the capability of on-demand reversible shape reconfigurations, desirable for many emerging applications (e.g., responsive metamaterials, soft robotics). Here, the design, fabrication, and modeling of soft electrothermal actuators based on laser-induced graphene (LIG) are reported and their applications in mechanically guided 3D assembly and human-soft actuators interaction are explored. Over 20 complex 3D architectures are fabricated, including reconfigurable structures that can reshape among three distinct geometries. Also, the structures capable of maintaining 3D shapes at room temperature without the need for any actuation are realized by fabricating LIG actuators at an elevated temperature. Finite element analysis can quantitatively capture key aspects that govern electrothermally controlled shape transformations, thereby providing a reliable tool for rapid design optimization. Furthermore, their applications are explored in human-soft actuators interaction, including elastic metamaterials with human gesture-controlled bandgap behaviors and soft robotic fingers which can measure electrocardiogram from humans in an on-demand fashion. Other demonstrations include artificial muscles, which can lift masses that are about 110 times of their weights and biomimetic frog tongues which can prey insects.

Strategically designed, well-defined 3D architectures could offer great opportunities, that are unavailable in their 2D counterparts, for a broad spectrum of applications, such as microelectronics, bioelectronics, photonics and optoelectronics, micro-electromechanical systems, metamaterials, energy storage and harvesting, soft robotics, and many others.^[1–22] Existing manufacturing techniques of 3D structures mainly include 3D printing, templated growth, fluidic self-assembly, and mechanically guided 3D assembly.^[1–22] Among these methods, the mechanically guided 3D assembly has recently attracted broad attention in the scientific community. The process starts from the planar fabrication of patterned 2D precursor structures, followed by the 2D-to-3D shape transformation via controlled rolling, folding, curving, and/or buckling.^[4] This process is naturally compatible with existing advanced planar fabrication technologies (e.g., lithographic and laser-processing techniques). Consequently, micro/nanoscale structures, sensors and/or other functional components

Y. Ling, X. Li, S. Goswami, Y. Liu, G. Zhao, B. Sun, Prof. G. Huang, Prof. Z. Yan
Department of Mechanical and Aerospace Engineering
University of Missouri
Columbia, MO 65211, USA
E-mail: yanzheng@missouri.edu

W. Pang, Z. Xu, Prof. Y. Zhang
Applied Mechanics Laboratory
Department of Engineering Mechanics
Center for Flexible Electronics Technology
Tsinghua University
Beijing 100084, China
E-mail: yihuizhang@tsinghua.edu.cn

 The ORCID identification number(s) for the author(s) of this article can be found under <https://doi.org/10.1002/adma.201908475>.

Z. Xu
The State Key Laboratory for Manufacturing and Systems Engineering
School of Mechanical Engineering
Xi'an Jiaotong University
Xi'an 710049, China

D. Stroman, Q. Fei, Y. Xu, Prof. Z. Yan
Department of Biomedical
Biological and Chemical Engineering
University of Missouri
Columbia, MO 65211, USA

Prof. J. Xie
Department of Surgery-Transplant and Mary
and Dick Holland Regenerative Medicine Program
College of Medicine
University of Nebraska Medical Center
Omaha, NE 68130, USA

DOI: 10.1002/adma.201908475

can be seamlessly integrated into 3D architectures in a pre-defined manner. Recent demonstrations include a 3D dome-like structure patterned with 48 MoS₂-based photodetectors, which can determine the power density and direction of the incident light,^[23] and 3D electronic scaffolds which can achieve multisite, simultaneous recording of field potentials from cocultured cardiac tissues.^[24]

The further development of mechanically guided 3D assembly requires the capability of controlled shape reconfigurations in an on-demand and reversible fashion, which is highly desirable for many emerging applications, such as responsive metamaterials, soft robotics, and tunable optics. Currently, many promising actuating materials, that can potentially trigger 2D-to-3D shape transformations, are available, such as dielectric elastomers, shape-memory polymers, polymer composites, and hydrogels, which can be driven by electricity, heat, light, magnetism, solvent, humidity, and/or multi-stimuli.^[25–39] For example, compressive bulking guided, on-demand 3D assembly has been recently achieved by using dielectric elastomers^[38] and shape memory polymers^[39] as the assembly substrates. However, these two strategies have some limitations in terms of high operation voltages (thousands of volts) and poor reversibility and cyclability, respectively. Among the existing actuation materials and mechanisms, electrothermal triggering in electroactive polymers is a very popular strategy, largely because of its easy fabrication and control, high reversibility and cyclability, low cost and operation voltages (tens of volts), and free use of electrolytes.^[25,26] However, most existing studies of electrothermally controlled 3D assembly lack a rational design method and assembly strategy of enabling 3D reconfigurations with complex geometries. Moreover, the interactions between human and soft actuators/robotics remain not well explored.

Besides, graphene is a promising functional material for pliable joule-heating elements in soft electrothermal actuators, due to its outstanding electrical, thermal, and mechanical properties.^[27] Recent research indicates that carbon dioxide (CO₂) laser treatment can convert various polymer films into porous graphene under ambient atmospheres, termed as laser-induced graphene (LIG).^[40] The transformation of polymers to LIG follows from a photothermal carbonization process that is enabled by localized high temperatures and pressures produced by laser irradiation, and the subsequent release of uncarbonized gas leads to the formation of porous structures.^[40] In addition, computer-controlled, motorized laser beams can make LIG patterns with arbitrary shapes on polymer films, such as polyimide (PI), in a pre-designed and high-precision manner, thereby providing a simple, efficient, and scalable approach of fabricating various graphene-based functional devices and components. Most recently, the applications of LIG in flexible electronics, artificial throats, supercapacitors, and bacterial air filters have been well explored.^[41–45] However, the studies in LIG-enabled, electrothermally controlled, mechanically guided 3D assembly are still limited.

In this paper, we report the design, fabrication, and modeling of LIG-based, soft, electrothermal actuators, and explore their applications in mechanically guided 3D assembly and human-soft actuators interaction. The actuators consist of the PI, LIG, and polydimethylsiloxane (PDMS) trilayer. LIG serves

as a pliable heater to introduce temperature differences via joule heating. The stress caused by the significant thermal expansion difference between PI and PDMS can deform strategically designed 2D precursors into programmed 3D architectures via global folding and/or local bending in a reversible and on-demand manner. More importantly, by using finite element analysis (FEA) as the design basis and incorporating ideas inspired by kirigami and origami, we have constructed more than 20 complicated, 3D architectures with pre-determined geometries. Notably, our research results indicate that FEA can quantitatively capture key aspects that govern electrothermally controlled, 2D-to-3D shape transformations, thereby providing a powerful tool capable of rapid design for versatile features. In addition, the fabrication of LIG actuators at an elevated temperature ($\approx 150^\circ\text{C}$) enables the realization of structures that can maintain their 3D shapes at room temperature without the need for electrothermal actuation. Furthermore, we demonstrate the interaction between human and LIG-based soft actuators. The two prototypic examples include i) responsive elastic metamaterials with human gesture-controlled bandgap behaviors; and ii) a soft robotic finger, with integrated bioelectronic sensors, which can wrap the human finger for electrocardiogram (ECG) measurements in an on-demand and reversible manner.

Figure 1 presents fundamental studies and comprehensive characterizations using U-shaped LIG actuators as the model example, which can serve as the basis for the design and construction of reconfigurable 3D architectures with complex geometries. The fabrication process is schematically illustrated in Figure 1a. The process begins with the direct CO₂ laser patterning of LIG as joule heaters on a commercial PI film (50 μm thick, Dupont) under ambient conditions. Cu wires are attached to the two ends of LIG heaters by silver epoxy for the connection to the power supply. Next, PDMS (Sylgard 184, Dow) is spin-coated on the sample surface and is thermally cured at $\approx 50^\circ\text{C}$. Cutting the sample into the pre-designed shape and dimension completes the fabrication of LIG actuators. The detailed fabrication process is described in the Experimental Section. Upon applying an actuation voltage, LIG heaters introduce temperature differences via joule heating. The stress caused by the significant difference in thermal expansion between PI and PDMS can induce bending deformations of the actuators toward the PI side. Here, PDMS and PI are selected as constituent materials, largely because of their large difference in the coefficient of thermal expansion, stability at a high operation temperature, and biocompatibility. Also, PI is an ideal precursor material for making LIG.^[40] The scanning electron microscope (SEM) image (Figure 1b) indicates that LIG has continuous, porous structures, which can facilitate the penetration of PDMS to strengthen the PDMS/LIG/PI interface and enhance the cyclability of the enabled actuators. The Raman spectrum of LIG (Figure 1c) shows a low D-to-G ratio (≈ 0.3), indicating the presence of few structural defects and high quality of the obtained graphene.^[46] This is further confirmed by LIG's low sheet resistance ($\approx 10\ \Omega\ \text{sq}^{-1}$), which is measured by a four-probe method. The calculated electrical conductivity of LIG is around $5000\ \text{S}\ \text{m}^{-1}$ based on the sheet resistance ($\approx 10\ \Omega\ \text{sq}^{-1}$) and thickness ($\approx 20\ \mu\text{m}$). And its thermal conductivity is about $0.6\ \text{W}\ \text{m}^{-1}\ \text{K}^{-1}$.^[47]

The largest bending angle accessible to LIG actuators represents an important parameter to evaluate the actuation

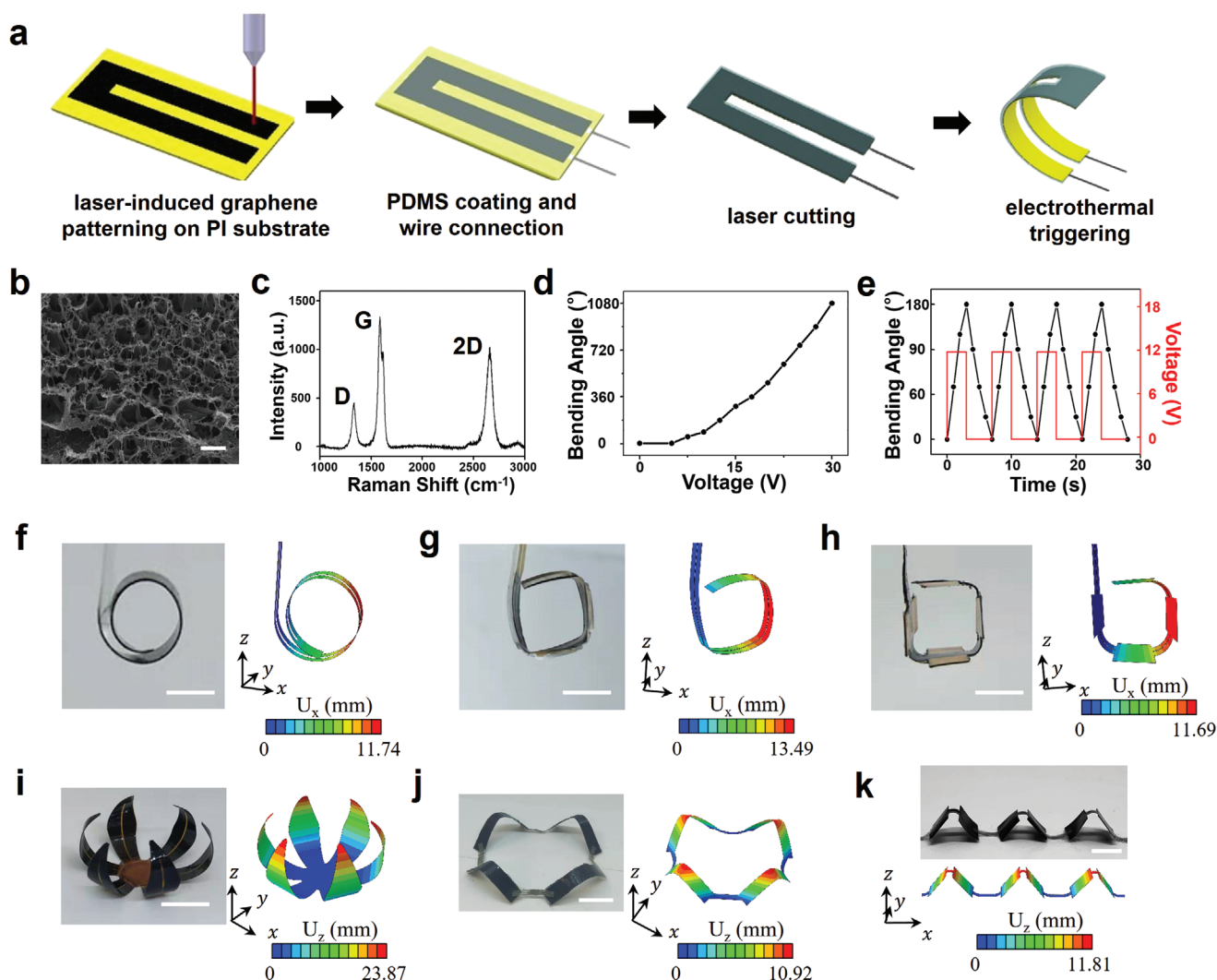


Figure 1. Fabrication, characterization, and modeling of LIG-based, soft electrothermal actuators. a) Schematic illustrations for the fabrication process. b) The SEM image and c) Raman spectrum of LIG. d) Actuation voltage dependence of the maximum bending angles of LIG actuators. e) Cyclic actuation and corresponding bending angle changes of LIG actuators driven by a 12 V square wave. Optical images and FEA predictions of f) ring-like and i) flower-like structures enabled by global bending, g) square-like and j) ring mountain-like structures enabled by origami-inspired local bending, and h) square-like and k) ridge-like structures enabled by kirigami-inspired local bending. The scale bars in (b) and (f–k) are 1 μm and 1 cm, respectively. The color bars of FEA results denote the distributions of two displacement components: U_x (along the x-axis) and U_z (along the z-axis).

performance. At prescribed input voltages, the maximum bending angles of LIG actuators can be largely affected by the modulus and thickness ratio of PDMS and PI. Here, the modulus of PI is fixed (2.5 GPa) and the modulus of PDMS can be tuned by adjusting the weight ratio of the base elastomer and curing agent. Based on FEA calculations and experimental measurements (Figures S1–S3, Supporting Information), the optimized thickness ratio of PDMS and PI can be determined. In this study, the spin-coated PDMS with a thickness of $\approx 200 \mu\text{m}$ and modulus of $\approx 2.5 \text{ MPa}$ is majorly used for the fabrication of soft actuators and construction of 3D structures, mainly based on the tradeoff of the maximum bending angle and fabrication feasibility. For given geometries and dimensions, the maximum bending angles of LIG actuators can be controlled by actuation voltages (Figure 1d and Figure S4, Supporting Information), which determine temperature differences

induced by LIG heaters. Here, well-designed LIG actuators can achieve the largest bending angle of 1080° and a bending curvature of 3.3 cm^{-1} ($\kappa = 1/R$, with κ being the bending curvature and R being the radius of curvature) at an actuation voltage of 30 V and 8 V sq^{-1} (Figure S5, Supporting Information), outperforming the previously reported ones.^[25–27] Moreover, the enabled LIG actuators exhibit outstanding reversibility and cyclability and can bend and unbend for over 1000 times without noticeable degradation of actuation performance (Figure 1e and Movie S1 and Figure S6, Supporting Information). After cycling 1000 cycles, the initiation of microcracks was observed only at very small regions of the interface (Figure S6c,d, Supporting Information). The actuator takes about 3 s to bend from 0° to 180° and about 4 s to recover, which are consistent with the heating time and cooling time provided by a square voltage wave (12 V for 3 s and 0 V for

4 s in one period). The LIG actuator allows for the demonstration of artificial muscles capable of lifting masses that are about 110 times of their weights (Movie S2 and Figure S7, Supporting Information), comparable to the recently reported, MoS₂-based, electrochemical actuators.^[34] Also, LIG soft actuators can be used to manipulate curvilinear objects, such as a wood cylinder (Movie S3 and Figures S8, Supporting Information).

As shown in Figure 1f, the actuator design with uniform thickness and cuts (as in Figure 1a) can only enable a global bending. Here, we exploit the design principles of origami (i.e., thickness control) and kirigami (i.e., cutting patterns control) to achieve the local folding of LIG actuators. In particular, we use CO₂ laser to thin PDMS layers on strategically selected locations to create creases on LIG actuators (Figure S9, Supporting Information). Upon actuation, LIG actuators can fold from crease regions to form pre-designed geometries (Figure 1g and Figure S10, Supporting Information). As demonstrated in Figure 1h, the local folding can also be realized by narrowing desired regions of LIG actuators using laser cutting. Figures 1i–k present three examples of electrothermally triggered shape transformations for forming flower-, ring mountain-, and ridge-like 3D structures, enabled by global bending, origami-inspired local folding, and kirigami-inspired local folding, respectively. In all of the different examples, the actuation deformations predicted by FEA agree well with the experiments, as evidenced by the close match of 3D configurations.

By using FEA as the design basis, the aforementioned approach can be further extended for the construction of a wide range of 3D architectures with highly diverse geometries. In addition to the shapes and numbers of LIG actuators, the patterns of origami creases and kirigami cuts can provide additional design options to expand the range of accessible 3D geometries. **Figure 2** summarizes experimental and computational studies of 19 representative 2D precursor designs that can transform into 25 pre-determined 3D shapes, each identified with a descriptive name, upon electrothermal actuation. Figure 2a provides four representative examples assembled through controlled rolling and bending deformations, which resemble a hanging bridge, semilunar wreath, crown, and tree silhouette. The electrothermally triggered 3D assembly is compatible with our recently developed, 3D assembly method guided by compressive buckling, in which 2D precursors, transferred onto prestretched elastomer substrates, are transformed into 3D architectures upon release of prestrain.^[12–19] As illustrated in Figure 2b,c, and Movies S4–S7 (Supporting Information), well-designed 2D precursors, mainly made of PI, are selectively bonded onto addressable LIG actuators. Depending on the 2D precursor design, the number of involved LIG actuators is from one to six. Upon electrothermal actuation, well-controlled bending of LIG actuators can deform 2D precursors into programmed 3D architectures. In the schemes of 2D precursors, red dots and yellow ribbons represent bonding sites and origami creases, respectively. Figure 2b provides 12 illustrative examples, including 3D structures that resemble an arched bridge, thorn basket, rotated table, rings table, umbrella, cage, double sphere, wings, triangular sunshade, box, pyramid, and hexagonal tent. Notably, for the six structures on the bottom of Figure 2b, the strategically designed origami creases are used to further guide the 3D assembly process to increase the geometric complexity.

The LIG actuators can be addressed independently in the 3D assembly, which can provide the unprecedented shape morphing capability inaccessible with previous methods. As illustrated in Figure 2c, and Movies S6 and S7 (Supporting Information), the flower stamen, epiphytic orchid and foldable quatrefoil can be reshaped into three distinct shapes, respectively, via sequential actuation of addressable LIG actuators. Besides, in this research, we mainly use PI as the basis material of 2D precursors for the capability demonstration. Similar to compressive bulking guided 3D assembly, electrothermally controlled 3D assembly is compatible with other functional materials, largely because the process starts from the planar form and the induced principal strains on the materials during the assembly process is dramatically minimized due to FEA-guided structural designs. This is further confirmed by the predicted principal strain distributions from FEA and *I*–*V* curves measured from LIG, patterned on the cage-like and rotated table-like structures, before/after 3D actuation, indicating negligible changes of the electrical conduction of LIG traces associated with these various shape reconfigurations (Figure S11, Supporting Information). For all the examples examined in Figures 1 and 2, the simulation results are in quantitative agreement with experimental results, demonstrating that FEA can serve as a reliable design tool for electrothermally controlled, mechanically guided 3D assembly with complex shapes.

The abovementioned LIG actuators can only bend from the flat state toward the PI side. Also, the enabled 3D structures are volatile at room temperature and revert to their initial shapes after the removal of actuation voltages. To broaden design options and application opportunities, we explore bidirectional shape transformations by strategically inducing thermal stress during the fabrication process (**Figure 3**). Specifically, the PDMS layers on LIG actuators are thermally cured at an elevated temperature (≈ 150 °C) as illustrated in Figure 3a. After cooling down to room temperature, PDMS contracts more than PI, due to its larger coefficient of thermal expansion, causing the bending of the actuator toward the PDMS side. As shown in Figure 3b, the enabled U-shape LIG actuator bends to around 360° toward the PDMS side at room temperature without actuation, becomes almost flat with 10 V actuation, and bends to around 300° toward the PI side with 20 V actuation. This capability can further broaden the design options of reconfigurable 3D structures. Figure 3c,d provides an illustrative example, which can maintain eight-petal-flower-like geometry at room temperature without actuation. This structure is almost flattened with 10 V actuation and is reshaped into a windmill-like structure with 10 V actuation voltage applied to the selected four petals and 20 V actuation voltage applied to the other four petals. In addition, a biomimetic frog tongue has been developed based on such novel types of LIG actuators. As shown in Figure 3e, and Movie S8 (Supporting Information), the biomimetic frog tongue rolls up at room temperature without actuation, unbends and elongates to capture a fly upon 20 V actuation, and reverts to the initial state after the removal of the actuation voltage.

Most recently, the interface of human and conventional machines (e.g., flying drones, robotics) has been explored.^[48–50] However, the studies in the interaction between human and soft actuators/robotics are still in the infant stage. As shown in

a							
Name	2D Precursor	3D Structure	FEA Simulation	Name	2D Precursor	3D Structure	FEA Simulation
Hanging Bridge				Crown			
Semilunar Wreath				Tree Silhouette			

b							
Name	2D Precursor	3D Structure	FEA Simulation	Name	2D Precursor	3D Structure	FEA Simulation
Arched Bridge				Thorn Basket			
Rotated Table				Rings Table			
Umbrella				Cage			
Double Sphere				Wings			
Triangular Sunshade				Box			
Pyramid				Hexagonal Tent			

c							
Name	2D Precursor	Shape I	FEA Simulation	Shape II	FEA Simulation	Shape III	FEA Simulation
Flower Stamen							
Epiphytic Orchid							
Foldable Quatrefoil							

Figure 2. Experimental and computational studies of a broad set of mechanically assembled, 3D structures triggered by electrothermal actuation. The 2D precursors, FEA predictions, and optical images of four 3D structures with a) mixed ribbons and membranes, b) twelve 3D structures bonded on LIG actuators, c) and three illustrative examples whose final geometries can be controlled via sequential actuation of addressable LIG actuators. In the schemes of 2D precursors, red dots and yellow ribbons represent bonding sites and origami creases, respectively. Scale bars: 1 cm.

Figure 4, and Movies S9 and S10 (Supporting Information), we provide two prototypic examples of human-soft actuators interaction, including the utility of human gestures to control LIG

actuators-based 3D shape morphing via real-time recording of electromyograms (EMG) and the utility of a soft robotic finger integrated with bioelectronic sensors for on-demand ECG

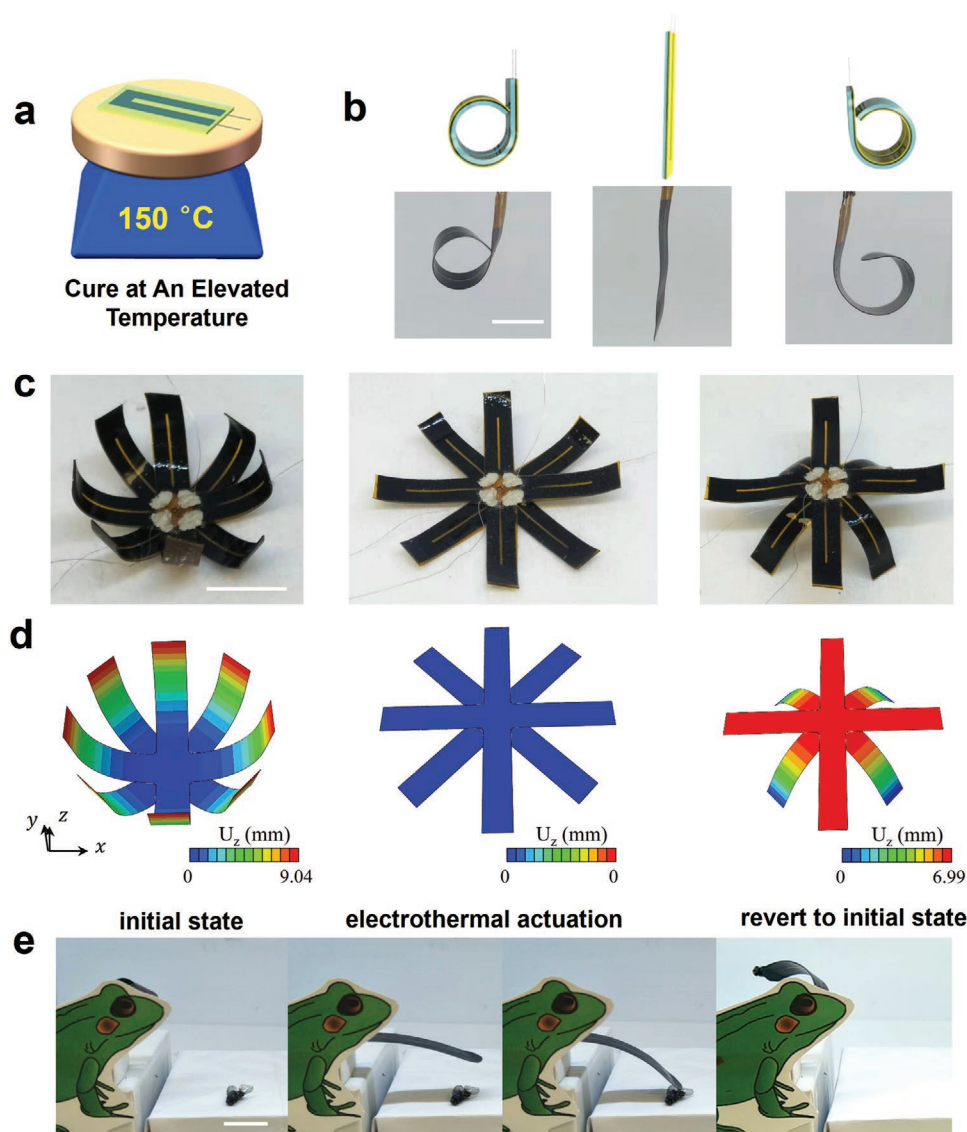


Figure 3. Experimental and computational studies of bidirectional shape transformation enabled by intentionally induced thermal stress during the fabrication process. a) The scheme of curing PDMS at an elevated temperature ($\approx 150\text{ }^{\circ}\text{C}$) to induce thermal stress on LIG actuators. b) A U-shaped LIG actuator, which bends to $\approx 360^{\circ}$ toward the PDMS side at room temperature without actuation, becomes flat with 10 V actuation, and bends to around 300° toward the PI side with 20 V actuation. c) The optical images and d) FEA predictions of a 3D structure, which can keep the 3D flower-like geometry at room temperature without actuation (left) and reconfigure into the flat pattern (middle) and windmill-like structure (right) upon electrothermal actuation. The color bars of FEA results denote the distributions of the displacements along the z-axis. e) A biomimetic frog tongue which can prey insects. Scale bars: 1 cm.

measurement from a human finger. As illustrated in Figure 4a, LIG-based wearable electrophysiological sensors were laminated on the forearm of a human volunteer (muscle: flexor carpi radialis) to record the relevant EMG signals when the volunteer performed three different hand gestures. The recorded EMG signals can be classified into three distinct command signals of LIG actuators to control the shape reconfiguration of a flower-like structure (Figure 4b and Movie S9, Supporting Information) and elastic metamaterials (Figure 4c,d). The flow chart is provided in Figure S12 (Supporting Information). By using LIG-based soft actuators as local resonators (Figure S13, Supporting Information), we realized a tunable elastic metamaterial beam working at ultralow frequency ranges (5–200 Hz).

A unit cell consists of a pair of LIG actuators bonded onto a host aluminum beam, serving as the local resonator, and is schematically illustrated in Figure S13a,b (Supporting Information). And the local resonator can be simplified as a mass-spring system (Figure S13c, Supporting Information). The resonance frequencies of a unit cell without and with actuation were measured with a 3D Laser Doppler Vibrometer and are provided in Figure S14 (Supporting Information). Without actuation, LIG actuators are flat and the first resonant frequency is at around 111 Hz. Upon electrothermal actuation, the first resonant frequency shifts to a lower frequency, around 51 Hz, due to the shape reconfiguration. This large tunability makes it a promising candidate for tunable vibration and noise

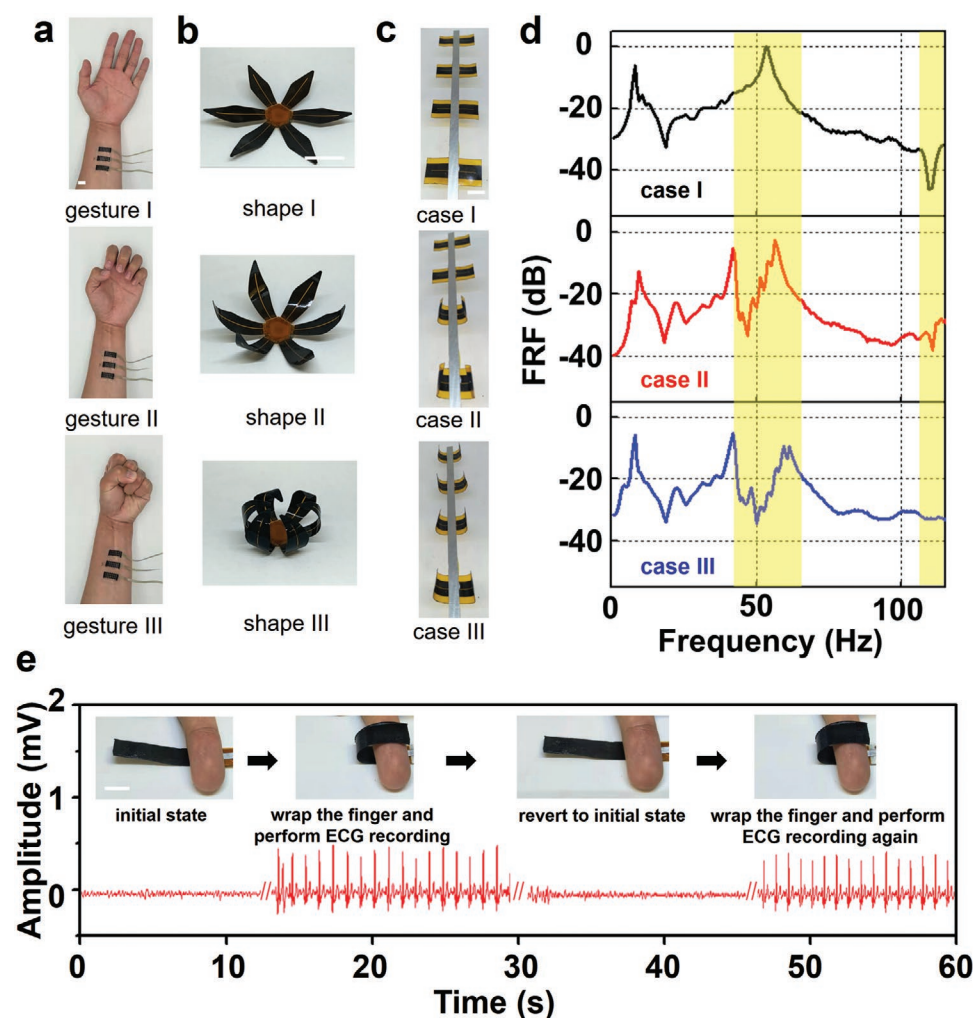


Figure 4. Demonstrations of human-soft actuators interaction. Via real-time EMG monitoring, a) human gestures are used to control the 3D assembly of a b) flower-like structure and c) shape reconfiguration of an elastic metamaterial for d) tunable bandgap behaviors. e) A soft robotic finger which can wrap the human finger for ECG measurement in an on-demand and reversible fashion. Scale bars: 1 cm.

control at ultralow frequency ranges.^[51,52] In the research, we fabricated elastic metamaterial by bonding four pairs of unit cells on a host aluminum beam, whose configurations can be controlled by human hand gestures (Figure 4c). A schematic of the experimental setup is provided in Figure S13d (Supporting Information). Specifically, we fixed one end of this metamaterial beam on a base and excited the base with a shaker. And a sweep sine signal (from 10 to 120 Hz) was amplified to excite the shaker. A 3D Laser Doppler Vibrometer was used to measure the frequency responses in the elastic metamaterial with different configurations (Figure 4d). In case I, all the unit cells remain flat and there is a dip near 111 Hz which is induced by the resonance of LIG actuators. In case III, the four pairs of unit cells are bent and the peak at around 51 Hz was largely attenuated. In case II, two pairs of the unit cells are bent and the other two remain flat. The bandgap behaviors, observed in cases I and III, were mixed in case II. Consequently, a tunable bandgap behavior is achieved at ultralow frequency regions. Furthermore, we developed a soft robotic finger integrated with LIG-based electrophysiological sensors (Figure S15a,

Supporting Information). The enabled soft robotic finger can warp the finger of a human volunteer for ECG measurements in an on-demand and reversible fashion (Figure 4e and Movie S10 and Figure S15b, Supporting Information).

In summary, we systematically study LIG-based, soft electro-thermal actuators through combined theoretical simulations and experimental validations, and explore their applications in mechanically guided, on-demand, reconfigurable 3D assembly, and human-soft actuators interaction. Using FEA as the basis of design optimization, more than 20 complex, 3D structures have been successfully constructed. The structures that can maintain their 3D shapes at room temperature without the need for electrothermal actuation are realized by strategically inducing thermal stress during the fabrication process. Furthermore, we demonstrate their applications in artificial muscles that can lift masses of about 110 times of their weights, a biomimetic frog tongue that can prey insects, elastic metamaterials with human gestures-controlled bandgap behaviors, and a soft robotic finger that can measure ECG signals from human fingers in an on-demand and reversible manner.

Experimental Section

Fabrications: The fabrication process of LIG actuators began with the direct CO₂ laser patterning of LIG on a commercial PI film (50 µm thick, Dupont) under ambient conditions. Here, LIG was made with a VLS2.30 universal laser system (wavelength: 10.6 µm, beam size: ≈120 µm, pulse duration: ≈14 µs, maximum power: 30 W, maximum scanning speed: ≈23 in. s⁻¹). The setting was fixed at 10.5% of the maximum power, 11% of the maximum scanning speed, and raster mode. The image density was set as 5. The pulse per inch was set as 1000. After LIG patterning, Cu wires were attached to the two ends of LIG patterns by silver epoxy for the connection to the power supply (Keithley 2604B). Next, PDMS (Sylgard 184, Dow) was spin-coated on the sample surface and thermally cured at ≈150 °C for the examples in Figure 3 and ≈50 °C for the examples in all other figures. The modulus of PDMS can be adjusted by controlling the weight ratio of the base elastomer and curing agent. The PDMS thickness can be controlled by the spin-coating speed. Finally, cutting the samples into pre-designed shapes and dimensions completed the fabrication of LIG actuators.

The 2D precursors in Figure 2b,c were fabricated by using the aforementioned CO₂ laser cutter. Here, the setting was fixed at 100% of the maximum power, 100% of the maximum scanning speed, and vector mode. The image density was set as 5. The pulse per inch was set as 1000. And the fabricated 2D precursors were bonded onto LIG actuators using adhesives. The LIG-based electrophysiological sensors in Figure 4a,e were fabricated using the recently reported procedures.^[41]

Characterizations and Measurements: The SEM image was taken with a FEI Quanta 600 FEG Environmental SEM. The Raman spectrum was collected with a Renishaw Raman microscope. Electrophysiological signals were recorded using PowerLab T26 (AD Instruments). The elastic moduli were obtained from a uniaxial tensile testing with a motorized tensile tester machine (Mark-10). The slope at the initial stage of the stress–strain curve was taken as the elastic modulus of the testing material. For each material, the modulus was determined based on the testing of five individual samples.

Finite Element Analysis: Finite element analysis was carried out using the commercial software ABAQUS to calculate the deformations of LIG actuators. Considering the ultrathin geometry, a composite bilayer (PDMS layer and PI layer) shell element was used to model the actuator, with refined meshes to ensure the computational accuracy. Due to the relatively small induced strains during bending/rolling deformations, the linear, elastic constitutive relations were employed for the two material components (PI and PDMS). The LIG layer, serving as the heating resource, was ignored in this model due to the porous internal configuration and low modulus of LIG. The orthotropic coefficient of thermal expansion of each material was exploited to predict orthotropic deformations. During the simulations, the temperature changes, measured with a commercial thermal camera (FLIR E6), were applied to the corresponding LIG regions of the shell model, which induce the thermal mismatch and result in the rolling deformations.

Experiments on Human Subjects: The in vivo evaluations of soft robotic fingers were conducted under the approval from the Institutional Review Board at the University of Missouri-Columbia (project number: 2 010 272). All human subjects gave written, informed consent before participation in the study.

Supporting Information

Supporting Information is available from the Wiley Online Library or from the author.

Acknowledgements

Y.L. and W.P. contributed equally to this work. Z.Y. acknowledges the financial support from the NSF grant (ECCS-1917630) and the

University of Missouri-Columbia start-up fund. Y.Z. acknowledges the support from the National Natural Science Foundation of China (Grant Nos. 11672152 and 11921002), the Tsinghua University Initiative Scientific Research Program (# 2019Z08QCX10) and the Tsinghua National Laboratory for Information Science and Technology. G.H. acknowledges support from the Air Force Office of Scientific Research under Grant No. AF 9550-18-1-0342 with Program Manager Dr. Byung-Lip (Les) Lee. The authors thank the technical support in the characterizations from “the Center for Nano/Micro Systems and Nanotechnology” at the University of Missouri-Columbia.

Conflict of Interest

The authors declare no conflict of interest.

Keywords

3D assembly, electrothermal actuators, human-soft actuators interaction, laser-induced graphene

Received: December 27, 2019

Revised: February 19, 2020

Published online:

- [1] J. A. Rogers, Y. Huang, O. G. Schmidt, D. H. Gracias, *MRS Bull.* **2016**, *41*, 123.
- [2] Y. Zhang, F. Zhang, Z. Yan, Q. Ma, X. Li, Y. Huang, J. A. Rogers, *Nat. Rev. Mater.* **2017**, *2*, 17019.
- [3] G. Huang, Y. Mei, *Small* **2018**, *14*, 1703665.
- [4] X. Cheng, Y. Zhang, *Adv. Mater.* **2019**, *31*, 1901895.
- [5] M. A. Skylar-Scott, J. Mueller, C. W. Visser, J. A. Lewis, *Nature* **2019**, *575*, 330.
- [6] H. Cui, R. Hensleigh, D. Yao, D. Maurya, P. Kumar, M. G. Kang, S. Priya, X. R. Zheng, *Nat. Mater.* **2019**, *18*, 234.
- [7] T. A. Schaedler, A. J. Jacobsen, A. Torrents, A. E. Sorensen, J. Lian, J. R. Greer, L. Valdevit, W. B. Carter, *Science* **2011**, *334*, 962.
- [8] Z. Chen, W. Ren, L. Gao, B. Liu, S. Pei, H. Cheng, *Nat. Mater.* **2011**, *10*, 424.
- [9] M. Y. B. Zion, X. He, C. C. Maass, R. Sha, N. C. Seeman, P. M. Chaikin, *Science* **2017**, *358*, 633.
- [10] Q. Liu, B. Xu, *Soft Matter* **2018**, *14*, 5968.
- [11] Z. Tian, L. Zhang, Y. Fang, B. Xu, S. Tang, N. Hu, Z. An, Z. Chen, Y. Mei, *Adv. Mater.* **2017**, *29*, 1604572.
- [12] Y. Liu, Z. Yan, Q. Lin, X. Guo, M. Han, K. Nan, K. C. Hwang, Y. Huang, Y. Zhang, J. A. Rogers, *Adv. Funct. Mater.* **2016**, *26*, 2909.
- [13] K. Nan, H. Luan, Z. Yan, X. Ning, Y. Wang, A. Wang, J. Wang, M. Han, M. Chang, K. Li, Y. Zhang, W. Huang, Y. Xue, Y. Huang, Y. Zhang, J. A. Rogers, *Adv. Funct. Mater.* **2017**, *27*, 1604281.
- [14] Z. Yan, F. Zhang, J. Wang, F. Liu, X. Guo, K. Nan, Q. Lin, M. Gao, D. Xiao, Y. Shi, Y. Qiu, H. Luan, J. Kim, Y. Wang, Y. Huang, Y. Zhang, J. A. Rogers, *Adv. Funct. Mater.* **2016**, *26*, 2629.
- [15] M. Han, H. Wang, Y. Yang, C. Liang, W. Bai, Z. Yan, H. Li, Y. Xue, X. Wang, B. Akar, H. Zhao, H. Luan, J. Lim, I. Kandela, G. A. Ameer, Y. Zhang, Y. Huang, J. A. Rogers, *Nat. Electron.* **2019**, *2*, 26.
- [16] H. Fu, K. Nan, W. Bai, W. Huang, K. Bai, L. Lu, C. Zhou, Y. Liu, F. Liu, J. Wang, M. Han, Z. Yan, H. Luan, Y. T. Zhang, J. Zhao, X. Cheng, M. Li, J. Lee, Y. Liu, D. Fang, X. Li, Y. Huang, Y. Zhang, J. A. Rogers, *Nat. Mater.* **2018**, *17*, 268.
- [17] Y. Zhang, Z. Yan, K. Nan, D. Xiao, Y. Liu, H. Luan, H. Fu, X. Wang, Q. Yang, J. Wang, F. Liu, L. Yang, H. Li, L. Wang, Y. Huang, J. A. Rogers, *Proc. Natl. Acad. Sci. USA* **2015**, *112*, 11757.

- [18] Z. Yan, F. Zhang, F. Liu, M. Han, D. Ou, Y. Liu, Q. Lin, X. Guo, H. Fu, Z. Xie, M. Gao, Y. M. Huang, J. Kim, Y. Qiu, K. Nan, J. Kim, P. Gutruf, H. Luo, A. Zhao, Y. Huang, Y. Zhang, J. A. Rogers, *Sci. Adv.* **2016**, 2, 1601014.
- [19] S. Xu, Z. Yan, K. Jang, W. Huang, H. Fu, J. Kim, Z. Wei, M. Flavin, J. McCracken, R. Wang, A. Badea, Y. Liu, D. Xiao, G. Zhou, J. Lee, H. U. Chung, H. Cheng, W. Ren, A. Banks, X. Li, U. Paik, R. G. Nuzzo, Y. Huang, Y. Zhang, J. A. Rogers, *Science* **2015**, 347, 154.
- [20] F. Liu, Y. Chen, H. Song, F. Zhang, Z. Fan, Y. Liu, X. Feng, J. A. Rogers, Y. Huang, Y. Zhang, *Small* **2019**, 15, 1804055.
- [21] Y. Liu, X. Wang, Y. Xu, Z. Xue, Y. Zhang, X. Ning, X. Cheng, Y. Xue, D. Lu, Q. Zhang, F. Zhang, J. Liu, X. Guo, K. Hwang, Y. Huang, J. A. Rogers, Y. Zhang, *Proc. Natl. Acad. Sci. USA* **2019**, 116, 15368.
- [22] Z. Fan, K. Hwang, J. A. Rogers, H. Huang, Y. Zhang, *J. Mech. Phys. Solids* **2018**, 111, 215.
- [23] W. Lee, Y. Liu, Y. Lee, B. K. Sharma, S. M. Shinde, S. D. Kim, K. Nan, Z. Yan, M. Han, Y. Huang, Y. Zhang, J. H. Ahn, J. A. Rogers, *Nat. Commun.* **2018**, 9, 1417.
- [24] A. Kalmykov, C. Huang, J. Bliley, D. Shiowski, J. Tashman, A. Abdullah, S. K. Rastogi, S. Shukla, E. Mataev, A. Feinberg, J. Hsia, T. Cohen-Karni, *Sci. Adv.* **2019**, 5, eaax0729.
- [25] L. Chen, C. Liu, K. Liu, C. Meng, C. Hu, J. Wang, S. Fan, *ACS Nano* **2011**, 5, 1588.
- [26] Q. Li, C. Liu, Y. Lin, L. Liu, K. Jiang, S. Fan, *ACS Nano* **2015**, 9, 409.
- [27] S. E. Zhu, R. Shabani, J. Rho, Y. Kim, B. H. Hong, J. H. Ahn, H. J. Cho, *Nano Lett.* **2011**, 11, 977.
- [28] Q. Ze, X. Kuang, S. Wu, J. Wong, S. M. Montgomery, R. Zhang, J. M. Kovitz, F. Yang, H. J. Qi, R. Zhao, *Adv. Mater.* **2019**, 31, 1906657.
- [29] J. Troyano, A. Carne-Sanchez, D. Maspoch, *Adv. Mater.* **2019**, 31, 1808235.
- [30] G. Wu, X. Wu, Y. Xu, H. Cheng, J. Meng, Q. Yu, X. Shi, K. Zhang, W. Chen, S. Chen, *Adv. Mater.* **2019**, 31, 1806492.
- [31] Y. Cheng, H. Lu, X. Lee, H. Zeng, A. Priimagi, *Adv. Mater.* **2019**, 31, 1906233.
- [32] C. M. Gomes, C. Liu, J. A. Paten, S. M. Felton, L. F. Deravi, *Adv. Funct. Mater.* **2018**, 28, 1805777.
- [33] C. Wang, K. Sim, J. Chen, H. Kim, Z. Rao, Y. Li, W. Chen, J. Song, R. Verduzco, C. Yu, *Adv. Mater.* **2018**, 30, 1804540.
- [34] M. Acerce, E. K. Akdogan, M. Chhowalla, *Nature* **2017**, 549, 370.
- [35] B. Jin, H. Song, R. Jiang, J. Song, Q. Zhao, T. Xie, *Sci. Adv.* **2018**, 4, eaao3865.
- [36] G. Cai, J. Ciou, Y. Liu, Y. Jiang, P. S. Lee, *Sci. Adv.* **2019**, 5, eaaw7956.
- [37] Y. Kim, H. Yuk, R. Zhao, S. A. Chester, X. Zhao, *Nature* **2018**, 558, 274.
- [38] W. Pang, X. Cheng, H. Zhao, X. Guo, Z. Ji, G. Li, Y. Liang, Z. Xue, H. Song, F. Zhang, Z. Xu, L. Sang, W. Huang, T. Li, Y. Zhang, *Natl. Sci. Rev.* **2020**, 7, 342.
- [39] J. K. Park, K. Nan, H. Luan, N. Zheng, S. Zhao, H. Zhang, X. Cheng, H. Wang, K. Li, T. Xie, Y. Huang, Y. Zhang, S. Kim, J. A. Rogers, *Adv. Mater.* **2019**, 31, 1905715.
- [40] J. Lin, Z. Peng, Y. Liu, F. Ruiz-Zepeda, R. Ye, E. L. Samuel, M. J. Yacaman, B. I. Yakobson, J. M. Tour, *Nat. Commun.* **2014**, 5, 5714.
- [41] B. Sun, R. N. McCay, S. Goswami, Y. Xu, C. Zhang, Y. Ling, J. Lin, Z. Yan, *Adv. Mater.* **2018**, 30, 1804327.
- [42] Y. Yang, Y. Song, X. Bo, J. Min, O. S. Pak, L. Zhu, M. Wang, J. Tu, A. Kogan, H. Zhang, T. K. Hsiai, Z. Li, W. Gao, *Nat. Biotechnol.* **2019**, 37, 378.
- [43] L. Tao, H. Tian, Y. Liu, Z. Ju, Y. Pang, Y. Chen, D. Wang, X. Tian, J. Yan, N. Deng, Y. Yang, T. Ren, *Nat. Commun.* **2017**, 8, 14579.
- [44] Z. Peng, R. Ye, J. A. Mann, D. Zakhidov, Y. Li, P. R. Smalley, J. Lin, J. M. Tour, *ACS Nano* **2015**, 9, 5868.
- [45] M. G. Stanford, J. T. Li, Y. Chen, E. A. McHugh, A. Liopo, H. Xiao, J. M. Tour, *ACS Nano* **2019**, 13, 11912.
- [46] L. Malard, M. Pimenta, G. Dresselhaus, M. Dresselhaus, *Phys. Rep.* **2009**, 473, 51.
- [47] M. K. Smith, D. X. Luong, T. L. Bougher, K. Kalaitzidou, J. M. Tour, B. A. Cola, *Appl. Phys. Lett.* **2016**, 109, 253107.
- [48] J. W. Jeong, W. H. Yeo, A. Akhtar, J. J. S. Norton, Y. J. Kwack, S. Li, S. Y. Jung, Y. Su, W. Lee, J. Xia, H. Cheng, Y. Huang, W. S. Choi, T. Bretl, J. A. Rogers, *Adv. Mater.* **2013**, 25, 6839.
- [49] B. Xu, A. Akhtar, Y. Liu, H. Chen, W. H. Yeo, S. I. Park, B. Boyce, H. Kim, J. Yu, H. Y. Lai, S. Jung, Y. Zhou, J. Kim, S. Cho, Y. Huang, T. Bretl, J. A. Rogers, *Adv. Mater.* **2016**, 28, 4462.
- [50] K. Sim, Z. Rao, Z. Zhou, F. Ershad, J. Lei, A. Thukral, J. Chen, Q. A. Huang, J. Xiao, C. Yu, *Sci. Adv.* **2019**, 5, eaav9653.
- [51] Z. Liu, X. Zhang, Y. Mao, Y. Y. Zhu, Z. Yang, C. T. Chan, P. Sheng, *Science* **2000**, 289, 1734.
- [52] K. Chuang, X. Lv, D. Wang, *Appl. Phys. Lett.* **2019**, 114, 051903.